

Design of a Head and Neck Restraint System for Use in City Cars

David HENDERSON, ZHOU Qing

(State Key Laboratory of Automotive Safety and Energy, Tsinghua University, Beijing 100084, China)

Abstract: City cars have various advantages in urban commuting and have become increasingly popular in Europe, Japan and China. However, due to their small size, city cars face significant challenge with collision protection. A new type of head and neck restraint was envisioned for providing similar motion control to that of race car systems but in such a way that it can be used in passenger cars. The concept of the design and its working principle were described in this paper. A rigid body model of the head restraint was developed to evaluate the requirements of an airbag inflator that can quickly deploy the system in a side impact and an energy analysis was used to comment on the feasibility of such a system. The results show that an airbag with a rate of pressure increase approximately four times that of a standard frontal airbag was sufficient to deploy the system within 15 ms. This new concept of head and neck restraint system will need further design and validation in application.

Key words: vehicle safety; city car; head restraint; deployment time; side impact

用于微型车的头颈约束系统的设计 (英文)

杨 刚 / David HENDERSON [英国], 周 青

(清华大学 汽车安全与节能国家重点实验室, 北京 100084, 中国)

摘 要: 微型车在城市通勤中有多种优势, 近年来在欧洲、日本和中国的使用不断在增加。另一方面, 由于尺寸小, 微型车的碰撞保护面临很大的挑战。本文开发了一种适用于普通汽车环境的新型头颈部约束系统, 旨在碰撞中实现类似赛车系统对头颈部运动的约束。给出了此头颈部约束系统的设计概念和碰撞保护原理, 建立了相应的刚体模型; 根据在侧碰过程中该头颈保护系统快速展开到位的要求, 进行了能量分析。结果表明: 当气囊以约 4 倍于前碰气囊的充气速度展开时, 驱动支撑于车顶的头颈保护系统, 可在 15 ms 以内到位。该新型头颈约束系统还需要进一步设计和验证, 才能应用。

关键词: 汽车安全; 微型车; 头部约束; 配置时间; 侧面碰撞

中图分类号: U 461.91 文献标识码: A DOI: 10.3969/j.issn.1674-8484.2016.03.002

收稿日期 / Received : 2015-11-01

基金项目 / Supported by : 中国 国家自然科学基金资助项目 (部分地) / National Natural Science Foundation of China (partly) (51675295)

第一作者 / First author : David HENDERSON (1986—), UK / 英国. E-mail: davidhenderson@126.com

第二作者 / Second author : 周青 (1964—), 美国籍, 教授. E-mail: zhouqing@tsinghua.edu.cn

Introduction

In the face of problems such as global warming, rapidly depleting fossil fuel reserves and worsening air quality, the need for cleaner vehicles has never been greater^[1]. Decreasing vehicle mass both reduces tire rolling losses and the energy lost during braking. Reducing vehicle mass therefore provides a method by which vehicle efficiency can be improved regardless of the powertrain employed.

This, together with the inconvenience that comes with driving a large car in a congested city with few parking spaces, has led many automakers to experiment with 'microcars' - small vehicles, usually electric, often with tandem seating, that typically have a mass half that of compact cars.

Despite the efficiency gains that the light weight of these vehicles brings, there are also serious safety implications for the occupants of such lightweight vehicles in the case of collision with a heavier vehicle. Studies based on empirical data have shown that the risk of fatality increases with the ratio of vehicle mass raised to the power of 3.8^[2].

Studies based on IndyCar race cars have shown that restraint systems which optimize body biomechanics during a crash have allowed occupants to survive much higher accelerations than the 60 g limit specified in FMVSS safety regulations^[3].

A seat design with more shoulder and hip restraint support and four-point seatbelts could conceivably be implemented on light-weight passenger cars to bring the level of safety closer to that offered by race car systems. However, the helmet and head restraint used in race cars is not a solution amendable to passenger cars.

In this paper, a new type of head restraint is presented that aims to bring to lightweight vehicles the same biomechanical advantages afforded by race car systems, without compromising driver comfort.

1 Tandem Seating

Microcars such as the Renault Twizy, Toyota i-road and VW L1 are all lightweight, two-seater vehicles with one seat in front of the other, instead of the more conventional side-by-side arrangement found in two-seater coupés. This tandem seating arrangement allows for a narrow vehicle width which offers advantages in manoeuvrability and parking and reduces aerodynamic losses. This seating arrangement also presents opportunities for new safety systems, since the space either side of the head is greater than that of a small city car. In this paper, a safety system is presented that takes advantage of this unusual seating arrangement to offer a superior level of head and neck protection in side and frontal crashes, compared to systems currently used in passenger cars.

2 Safety Principles

The following section provides an overview of the principles of operation behind current safety systems and the limitations of

these components.

2.1 Airbags

Modern passenger cars come with a three-point seat belt and frontal airbag as standard safety features. Airbags have been shown to be effective at reducing the level of injury in severe crashes^[4]. In addition to absorbing occupant kinetic energy, the airbag reduces neck loading and reduces the magnitude of rotational acceleration of the brain which is believed by many researchers to be more important than translational acceleration in causing brain injury^[5].

However, the safety and efficacy of airbags is highly dependent on the distance between the driver's body and the airbag at the time of deployment. Occupants positioned too close to the steering wheel can suffer serious injuries upon airbag deployment which in some cases can be fatal^[6]. These limitations are due in part to the large variation in occupant size and seating position but are also due to the nature in which the airbag inflates, with lower inflation speeds and smaller airbag volume linked to a lower incidence of injury^[7]. In the case of a Formula One race car, where the occupant position is well defined, a highly optimized airbag can be developed. Such an airbag has been shown to be highly effective, matching the performance of the head and neck restraint (HANS) mandated for use in all races today^[8].

2.2 Lateral Support

Existing airbags and seat belts provide little control of the relative motion between the pelvis, shoulders and head, especially in the case of side and off-centre frontal collisions.

This is important for two reasons. Firstly, in cases where there is little or no lateral constraint at the shoulders, there is a risk of contact with interior surfaces of the vehicle. This is significant since more than 95% of cases of diffuse axonal injury, a severe form of brain injury commonly seen in severe head injuries resulting from car crashes, have been associated with head contact with interior surfaces^[9]. Secondly, in the case where the shoulders are constrained by side supports and no contact is made between the head and interior surfaces, the head must be decelerated by structures in the neck and spine. High tensile forces in the neck can cause fatal injuries such as basilar skull fracture and spinal dislocations^[10]. Indeed, in IndyCar races, basilar skull fracture was a frequent cause of death before 2001 when the HANS restraint was mandated^[11].

Increasingly, side air bags are being used to improve safety during a side impact. Side air bags provide a cushion between the door and the occupant's head to reduce head acceleration and repel shattered glass fragments. However, side airbags cannot provide control of neck motion during rebound and do not offer any protection in the case of a side impact on the opposite side of the car or in the case of an oblique collision, where the motion of the occupants head, relative to that of the car, is towards the A-pillar, missing the side and frontal

airbags.

In some race cars, supports either side of the head form part of the seat structure and offer protection to the head and neck during side collisions. Side impact tests at 45 g using a seat fitted with pelvis, shoulder and head supports that yield plastically have demonstrated that increasing the stiffness of the supports, such that they do not yield, can reduce neck loading from 4 kN, close to the limit of the onset of basilar skull fracture, to less than 1 kN by limiting neck motion^[3]. These side supports also prevent the head from colliding with interior surfaces of the vehicle.

3 Design Requirements

For the reasons outlined in the previous section, a head restraint design that can reduce neck loading and rotational acceleration of the brain whilst also preventing contact with interior surfaces of the vehicle will reduce the risk of head injury in high acceleration crashes where the shoulders and pelvis of the occupant are rigidly constrained, as in the case of a seat with shoulder and pelvis supports.

In order to ensure the design can accommodate all occupants, consideration must be given to the variation in human anthropometry and the range of possible seating positions. A head restraint designed for microcars must also satisfy the comfort and aesthetic requirements of users. Like an airbag, the system should be invisible and unobtrusive to the user until a crash event occurs.

The requirements of the system can be summarised as follows;

- Provide a means to restrict sideways and forward head motion.
- Maintain an optimal distance between airbag surface and occupant face.
- Suit a range of occupant head sizes, statures and seating positions.
- Remain invisible to the user until triggered.
- Total width of the system must be less than 1.2 m to be used in microcars.

4 Design Concept

Several design concepts were evaluated against the requirements listed above. Ultimately, the concept that was chosen uses rigid plates lined with energy absorbing foam that are stored horizontally in the roof of the vehicle.

These plates rotate 90° during a crash to form two vertically orientated side supports either side of the head. In addition, they form a support structure for the frontal airbag, as shown in Figure 1.

The airbag is also stored in the roof and inflates downwards to occupy the space between the plates. The airbag is supported at its rear surface by a support web of criss-crossing cables that

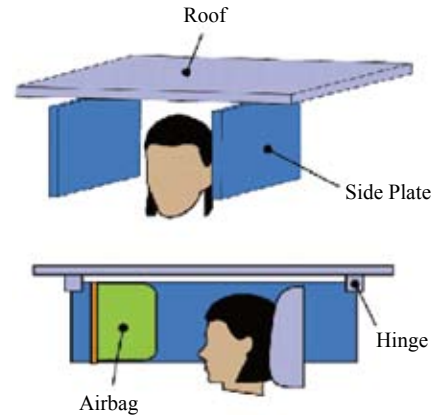


Figure 1 Side Plates and Airbag in Deployed Position

span between the two side plates.

The side plates are deployed under the force provided by two smaller side airbags. The side plates are constrained in their vertical position by high strength cables and the airbag support web. A simple schematic of the deployment process is shown in Figure 2.

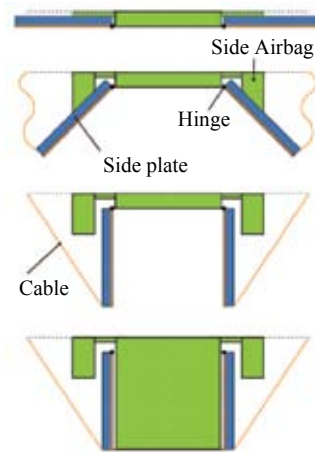


Figure 2 Side Plate and Airbag Deployment Process

4.1 Anthropometric Considerations

4.1.1 Side Plate Spacing

The Society of Automotive Engineers (SAE) J1052 standard gives head position contours for a 99th percentile male^[12]. To avoid risk of injury from premature contact, the side plates must not enter the envelope of motion defined by these contours during deployment.

Conversely, if the side plates are positioned too far from the head position envelope, there is a risk that the safe limit of lateral neck rotation will be exceeded before contact with the side plates is made. In the case of the 99th percentile male, the

gap between shoulders and shoulder supports will be minimal and therefore the distance between the side of the head and the lateral support structure will mostly be traversed by motion of the head relative to the base of the neck.

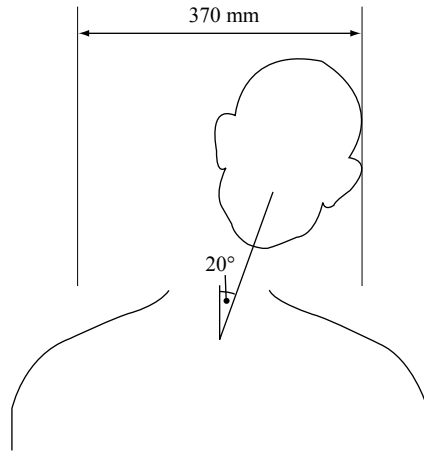


Figure 3 20° of Head Rotation for 99th Percentile Male

Experiments with volunteers give a range of non-injurious neck rotation, relative to the base of the neck (T1 vertebra) as 24°~37°. Limiting neck rotation to 20° is therefore taken as a constraint in this design^[13].

For a 99th percentile male, a lateral neck rotation of 20° is reached with a side plate spacing of 370 mm. Since the width of the 99th percentile male head contour is less than 370 mm, the actual side spacing will be set in accordance with the head contour for 99th percentile male: 166.79 mm on the inboard side and 189.79 mm on the outboard side - a total of 356.58 mm.

4.1.2 Side Plate Height

Sitting height for a 99th percentile male is 991 mm and the difference in sitting height and shoulder height is 327 mm^[14]. Allowing for the 133.5 mm clearance between the top of the occupants head and the roof specified in SAE J1052, a side plate height of 400 mm would provide ample overlap with the sides of the head. A constant height side plate cannot provide sufficient overlap for occupants of all sizes, however. In the case of a 1st percentile female, with a sitting head height of 774 mm, the overlap with a 400 mm side plate would be just 49.5 mm. A variable height side plate can be used to overcome this problem, since shorter people will sit closer to the front of the vehicle in order to access the controls.

The seat track length can be found from a consideration of the hip joint locations for a range of occupant sizes, such that they can reach the accelerator pedal. SAE standard J4004 gives the hip joint locations, from which a track length of approximately 240 mm is obtained^[15].

For a typical passenger car, the seat back angle ranges from

20°~26° or 22°~28° for a sports car^[15]. Some seat designs allow for a minimum angle of 10°^[16]. A range of 10 to 28 degrees angle will therefore be used in this analysis to ensure all user cases are covered.

With the side plates stowed in the roof, the total width of the system of the system is given by the sum of the height of the two side plates and the 356.58 mm space between them. To keep the total system width below the 1,200 mm specified in the design requirements, the seat track is angled. As the seat is moved forward, the seat height increases slightly. The side plate height can be reduced further by lowering the rotation joints so that they are offset from the roof.

A side plate design that gives a total system width of 1,057 mm is shown in Figure 4 along with a range of extreme occupant positions.

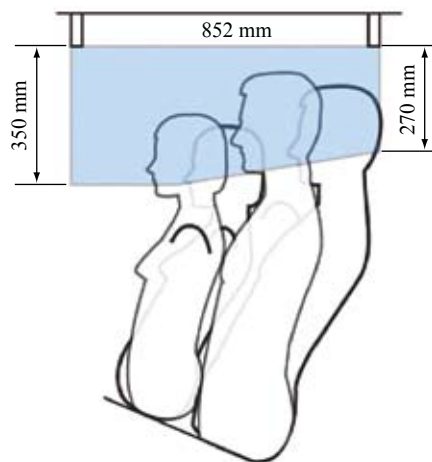


Figure 4 Side Plate Dimensions and Occupant Positions

4.1.3 Airbag

Studies of head and neck kinematics during frontal impacts using sled tests with volunteers have shown that the absolute motion of the head can be approximated as a phase of horizontal translation followed by a rotation^[17]. A typical plot for a volunteer test with a double vertical strap seat belt is shown in Figure 5.

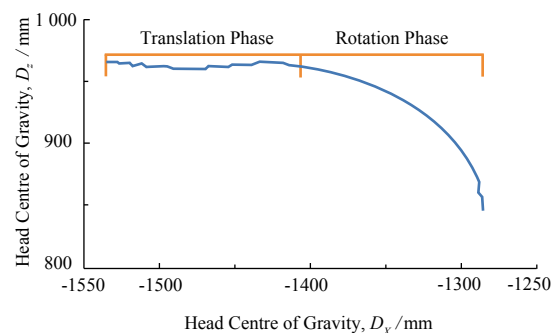


Figure 5 Absolute Motion of Head During Frontal Impact Sled Test

The displacement of the head during the translation phase depends mostly on the slack and stiffness of the seat belt. Ideally, the head makes contact with the airbag just before the rotation phase. In this way, the head can be decelerated over a greater period of time and head rotation can be minimised. Knowing the seat belt slack, seat belt stiffness and an approximation for thorax compliance, the displacement of the translational phase can be estimated. Based on volunteer tests with a double vertical strap seat belt, typical values fall in the range 100~150 mm^[17]. A value of 125 mm will therefore be used as the ideal initial spacing between the surface of the airbag and the face of the occupant.

As can be seen from Figure 4, the distance between the face of a 1st percentile female occupant sitting with a 10° seat back angle and a the face of a 99th percentile male sitting with a seat back angle of 28° is approximately 350 mm. An airbag mounted within the steering wheel must be designed such that it will not contact the face of the first percentile female occupant during deployment. As such, the design will be sub optimal for larger occupants. In the case of the 99th percentile occupant with a double strap seatbelt, it is conceivable that the head would miss the airbag completely.

In this design, the airbag is mounted in the roof of the vehicle and is free to move forwards and backwards between the side plates. The airbag is supported at its rear surface by a webbing which spans between two mobile carriages attached to the plates, as shown in Figure 6.

The position of the mobile carriages is controlled by a motor driven ball-screw as shown in Figure 7. The position is updated according to the position of the seat head rest which is inferred from the seat back angle and seat track position.

In this way, a spacing close to 125 mm can be maintained between the front airbag surface and the face of the occupant. A more advanced system could use optical sensors to

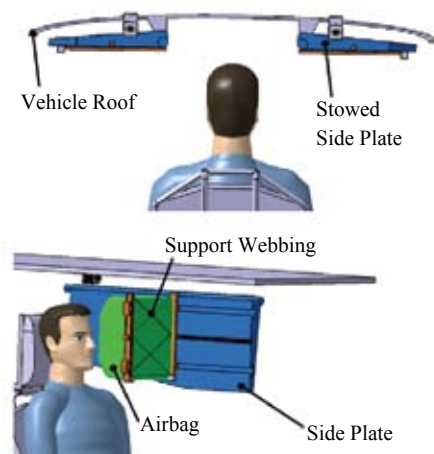


Figure 6 3-D Model of Head Restraint in Stowed and Deployed Position with Right Side Plate Hidden to Show the Airbag Support Structure

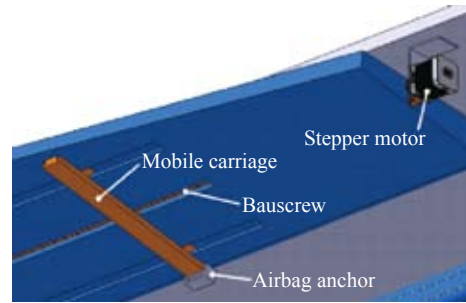


Figure 7 3-D Model of the Side Plate in Stowed Position Showing the Stepper Motor Driven Ballscrew and Slider

determine head position more accurately. Conversely, a cheaper implementation could use a direct mechanical link between the mobile carriages and head rest.

The total space between the head rest and the rear surface of the airbag is the sum of the airbag depth, the 125 mm of spacing and occupant head length. Since occupant head length will generally scale with occupant stature, there may be merit in adjusting the spacing according to seat track position. In this design, for simplicity, a fixed head length of 200 mm is used. For airbag depth, a value of 150 mm is used as this was found to work well in another airbag design^[8]. A schematic showing the deployed airbag for the two extremes - a 1st percentile female with a 10° seat back angle and a 99th percentile male with a 28° seat back angle - is shown in Figure 8.

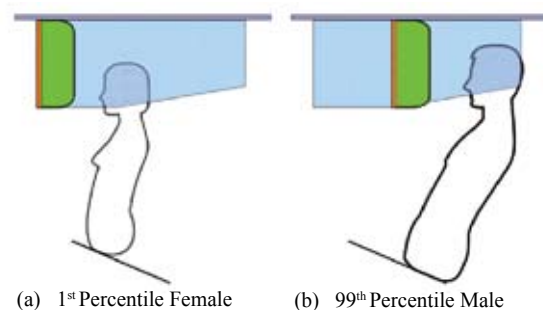


Figure 8 Airbag Positions for Occupants

4.2 Dynamic Considerations

Airbags of various shapes and sizes have been developed with success^[18]. Airbags, by virtue of their lightweight, are quick to deploy. Rigid side plates have significantly higher mass and therefore the feasibility of deploying them in the tight time window of a side impact must be assessed.

4.2.1 Deployment Time

The time event profile for a side impact derived from a lumped-mass model is shown in Figure 9.

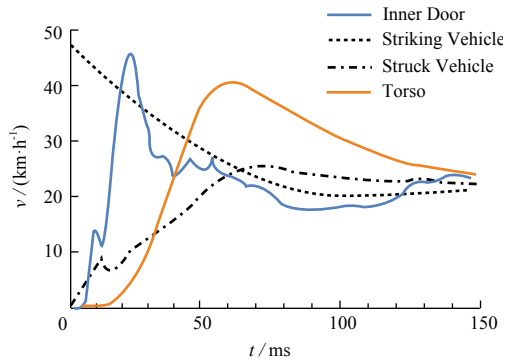


Figure 9 Velocity Profile for Side Impact, Adapted from Ref. [19]

The occupant torso starts gaining speed around 20 ms and accelerates steeply after 25 ms. The side supports must therefore be in place before 20 ms has elapsed. The time taken for the sensing algorithm to detect a side impact is approximately 5 ms [20]. The remaining time available for deployment is therefore 15 ms.

4.2.2 Material Selection

Studies on IndyCar race cars have found that occupants have survived side impact crashes without injury at chassis accelerations of 120 g [3].

Using this as an approximation for the maximum acceleration seen by the side plates, the maximum loading force can be estimated by multiplying this acceleration by the mass of the occupant's head. The head and neck mass for the 95th percentile male Hybrid III dummy is 6.65 kg [21]. The maximum loading force can therefore be estimated as 7.82 kN.

In addition to supporting this force, this side plate must also be capable of sustaining the airbag load without significant deformation. The moments generated in the side plate due to the airbag force can be eliminated by applying the airbag force over the entire area of the side plate.

In its deployed state, the side plate effectively forms a simply supported plate loaded with a point load at the head contact point. Modelling the side plate as a simply supported beam with a load at its centre provides a means by which the effect of material and geometry changes can be assessed.

The minimum required plate thickness for the maximum head force, h , can be obtained from simple beam theory,

$$h = \sqrt{\frac{3P}{2\sigma}},$$

where P is the load from the head and σ is the yield stress of the side plate material.

The force required to accelerate the plates into position is provided by the pressure generated in the side deployment airbags. Assuming the force is constant during deployment and neglecting losses, the equation of motion of the plate can be written as:

$$I\ddot{\theta} = F_a x,$$

where x is distance between plate rotation axis and point of application of force, $\ddot{\theta}$ is the angular acceleration of the side plate, about the rotation axis, F_a is the force applied on the side plate by the deployment airbag and I is the moment of inertia about the rotation axis given by

$$I = \frac{\rho b h l}{3} (b^2 + h^2),$$

where ρ is the material density, b is the side plate height and l is side plate length. The airbag force, $F_a = f(t)$, depends on the pressure generated within the plate deployment airbag multiplied by the projected area in the z direction. An airbag area of 852 mm by 350 mm is used in this analysis.

A pressure-time profile for a typical frontal airbag is shown in Figure 10 along with a second-order polynomial approximation of the data.

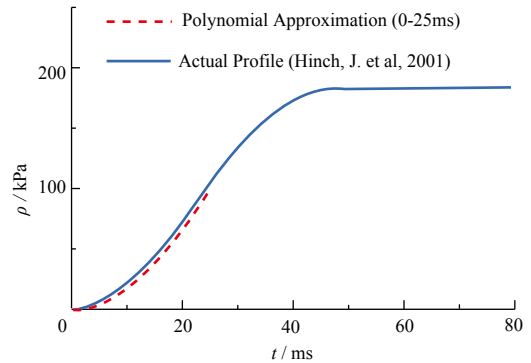


Figure 10 Pressure Profile for Typical Frontal Airbag. Adapted from Ref. [4]

This pressure profile can be scaled by a factor K to simulate the effect of using a larger inflator. K represents how many times greater a rate of pressure increase is required, compared to the baseline pressure profile. The airbag force can thus be written as;

$$F_a = Kp(t)A = KA(a_1 t^2 + a_2 t + a_3).$$

A quick estimate of the effect of material on the value of K can be obtained with the simplified equation of motion. Integrating twice over the range $\theta = 0$ to $\theta = \pi/2$ gives the relationship between K and I as:

$$I = \frac{KAx}{\pi/2} \left[\frac{a_1 t^4}{12} + \frac{a_2 t^3}{6} + \frac{a_3 t^2}{2} \right]_0^{1.5 \text{ ms}}.$$

Evaluating h and I for a range of materials gives the plot shown in Figure 11.

In reality, the required scale factor will be larger than that shown here since the airbag force will reduce as the plate rotates. Nevertheless, this simple analysis clearly shows that metallic materials require an inflator with at least seven times greater rate of pressure increase than the baseline frontal

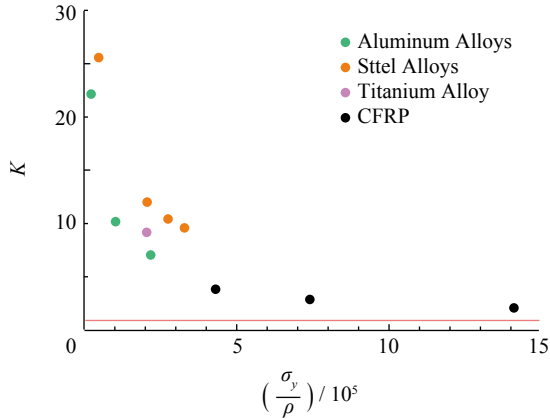


Figure 11 Required Scale Factor, K , for a Range of Materials [22-23]

airbag. Carbon fibre reinforced polymer (CFRP) requires a much lower scale factor. For this reason, CFRP was chosen as the material for this design.

4.2.3 Pressure Profile

With the material and inertia of the side plate determined, the effects of a varying airbag force and aerodynamic drag can now be included to give the deployment time and the required airbag pressure profile.

The side deployment airbags inflate downwards to a height, z_{lim} , beyond which the airbags and plates separate. The plates then continue rotating, with some slowing due to aerodynamic losses. Retardation due to losses in the bearings are neglected since the mass of the plate is relatively small. A force diagram for the plate-airbag interaction is shown in Figure 12.

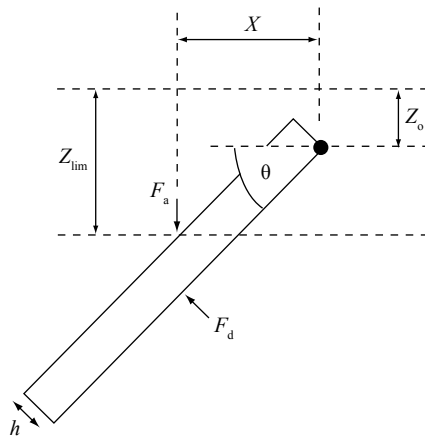


Figure 12 Force Diagram for Deploying Side Plate

The full equation of motion, including aerodynamic drag, can be written as;

$$I\ddot{\theta} = xF_a \cos\theta - \frac{b}{2}F_d,$$

where F_d is the aerodynamic drag force and θ is the angle of

plate rotation.

This equation is valid for the period during which the airbag is in contact with the plate. The geometric parameters used in this analysis are given in Table 1.

Table 1 Side Plate Model Parameters

x	perpendicular distance between plate rotation axis and point of application of force	150 mm
h	side plate thickness, at point of contact with airbag	determined by material
z_0	initial z displacement of side plate, at point of contact with deployment airbag	30 mm
z_{lim}	average z displacement of deployment airbag when fully deployed	200 mm

The aerodynamic force was estimated using the following formula;

$$F_d = \frac{1}{2} \rho C_d \int u^2 dA = \frac{1}{2} \rho C_d l b^3 \dot{\theta}^2,$$

where C_d is the drag coefficient, taken to be 1.5, A is area of the side plate, ρ is the density of air and $\dot{\theta}$ is the angular speed of the side plate.

Modelling this equation in Matlab with CFRP as the side plate material gives a required scale factor of 4. Figure 13 shows the plate rotation plotted against time.

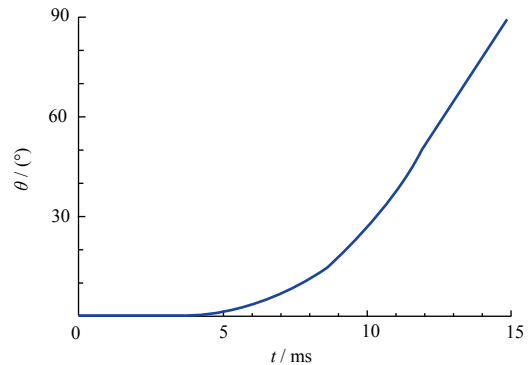


Figure 13 Side Plate Rotation, Plotted against Time

5 Finite Element Analysis of Design Concept

The aim of the above analysis was to quickly assess the feasibility of deploying the side plate with an airbag in the short time required. Several assumptions were made that together could cast doubt on the results.

The first of these assumptions is that the side plate can be modelled as a simply supported beam. The required thickness of the beam is calculated using simple beam theory and this is then used to calculate the rotational moment of inertia. The

inaccuracies in this assumption will therefore also affect the accuracy of dynamic model prediction. The second assumption is that the rate of pressure increase for the airbag pressure profile can be scaled up. It is further assumed that the pressure profile is not changed by the interaction with side plate.

As an additional check, two further analyses will be performed:

- 1 a finite element analysis of head impact with the side plate to assess whether or not the side plate thickness estimated by the beam theory calculation is sufficient;
- 2 an energy conservation based calculation as an additional check that the system is feasible.

5.1 Side Plate-Head Impact Response

In the above analysis, the side plate was modelled as a simply supported beam. Modelling the side plate in this way allowed for easy manipulation of the geometrical and material properties, but it is likely to have introduced significant errors in the calculation. The aim of this section is to estimate the size of such errors and assess their impact on the validity of the result.

A finite element analysis (FEA) was performed in ANSYS to evaluate the plate deformation and stress under a point load of 7.82 kN at the centre of the plate. This is representative of a head impact during side a side collision that leads to a peak acceleration of 120 g. In the case of a frontal collision the side plates will also be loaded via the airbag, through the mobile carriages. Since the mobile carriages load both plates, through multiple contact points, it is reasonable to assume that this loading condition will be less severe than a side head impact in which just one plate is loaded at a single location. The case of loading through the mobile carriages is therefore not included in this simple analysis.

A simple rectangular plate of dimensions 852 mm by 350 mm was used in the model. The simply supported beam model used in the previous analysis gave a required thickness of 3.1mm. This was the plate thickness used in the FEA.

The hinge joint was represented in the model by constraining all degrees of freedom of the bottom edge of the plate, except for x-axis rotation. To represent to effect of the steel cables preventing plate rotation, the outer edge faces were constrained to prevent translation in the y-axis direction. All other degrees of freedom were free. These boundary conditions are illustrated in Figure 14.

The contact stress at the point of load application will be sensitive to the size of the contact patch. This depends on the radius of curvature of the contact surfaces and the material properties of the two bodies in contact. The assumption is made that the material does not yield at the contact point (i.e. the head does not penetrate the plate). In order to justify this assumption, the contact stresses in the case of skull contact with the plate will be estimated. In reality, the skin covering of the skull and the compliant energy absorbing foam layer will

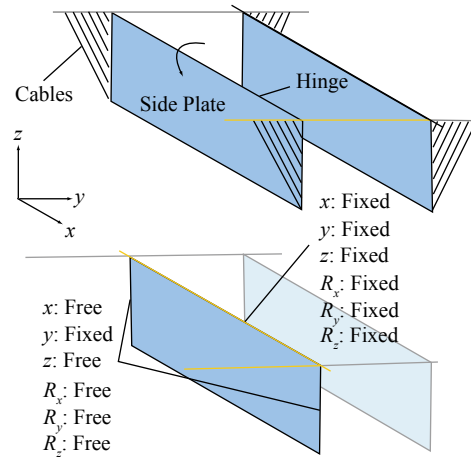


Figure 14 Boundary Conditions Applied in Model

help distribute the force upon impact but to give an estimate for the worst case, these contributions are not considered in the analysis that follows.

The skull is modelled as a bone sphere of constant radius 75 mm, Poisson's ratio 0.22, and elasticity modulus 15 GPa^[24]. The side plate is modelled as a perfectly flat surface with Poisson's ratio 0.31 and elasticity modulus 9.5 GPa^[25]. The radius of the contact patch for the contact between an elastic sphere and elastic plate was derived by Hertz^[26] and can be written as:

$$a = \sqrt[3]{\frac{3FR^*}{4E^*}},$$

where F is the contact force, E^* is the reduced elasticity modulus:

$$\frac{1}{E^*} = \frac{1-\nu_1^2}{2E_1} + \frac{1-\nu_2^2}{2E_2},$$

and R^* is the reduced radius of curvature:

$$\frac{1}{R^*} = \frac{1}{R_x} + \frac{1}{R_y}.$$

Substituting the values gives $E^* = 12.6$ GPa, $R^* = 37.5$ mm and a contact patch radius of 2.6 mm. In the FEA, the force will be applied to all surface nodes within a 2.6 mm radius of the contact point. In the case of sphere-plate contact, the peak pressure is given by the following equation;

$$P_{max} = \frac{3F}{2\pi a^2}.$$

Evaluating this equation with the values given above gives a peak contact stress of 552 MPa. This is below the yield stress of the material (1.1 GPa) so even in the case of bare bone and plate contact, the plate will not yield locally.

The plate was meshed with 5 mm quad elements. Experimentation with mesh size found this to be a suitable level of resolution - further decreases in mesh size had little effect on the results.

The von-Mises stress distribution is shown in Figure 15.

The stress is highest around the point of contact. This is thought to be an artefact associated with the point load. Even if this high stress is discounted, the stresses at locations distant from the contact point are in excess of the ultimate tensile stress of the carbon fibre plate — 1.1 GPa. This suggests that the simple beam model has underestimated the plate stress and therefore the required plate thickness.

A modified plate was created, with variable thickness geometry and support ribs, as shown in Figure 16.

The von-Mises stress distribution for the modified plate is as shown in Figure 17.

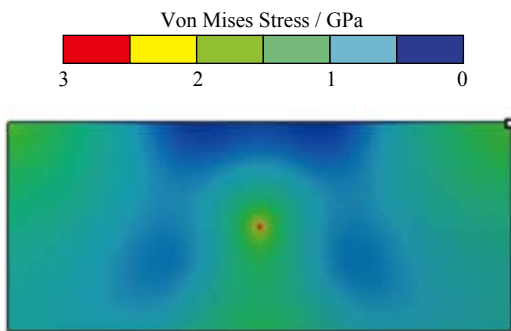


Figure 15 Von-Mises Stress Distribution

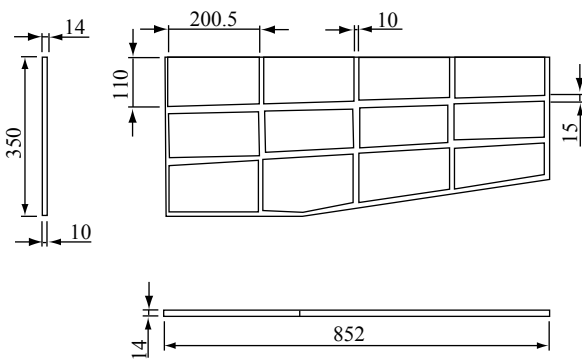


Figure 16 Geometry of Modified Side Plate

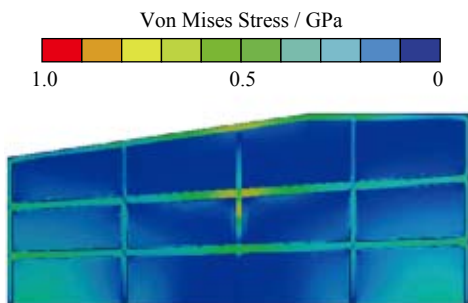


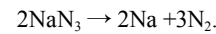
Figure 17 Von-Mises Stress Distribution for Modified Plate Geometry

The maximum stress was reduced to 900 MPa with this new plate geometry. Maximum plate deformation was reduced to 27 mm.

Despite an increase in mass of 50%, a distribution of mass closer to the hinge led to a rotational inertia of 0.067, only 10% higher than the previous side plate (0.0613). Re-running the side plate dynamic Matlab model with the increased moment of inertia and adjusting the K-value such that deployment time is 15 ms gives a new K-value of 4.4 (increased from 4). With the modified geometry, the side plate is therefore sufficiently strong to resist a head contact load of 7820 N without yielding and with only 16 mm of deflection at the head contact point.

5.2 Energy Considerations

A typical airbag, when triggered, fills up with nitrogen gas produced by a rapid chemical reaction. Sodium azide is the material usually used for this purpose. The sodium azide decomposes to form nitrogen and sodium via the following reaction:



The standard enthalpy of formation of sodium azide is 70.2 kJmol⁻¹ [27]. The enthalpy change of the reaction is therefore;

$$2(\Delta H^\circ_f)_{\text{Na}} + 3(\Delta H^\circ_f)_{\text{N}_2} - 2(\Delta H^\circ_f)_{\text{NaN}_3} = 140.4 \text{ kJ mol}^{-1}$$

The molar mass of sodium azide is 65 g mol⁻¹. The energy released per mass is therefore 2160 kJ kg⁻¹.

The side plate starts at rest and reaches maximum velocity at the point when the airbag and plate separates. Neglecting work done against air resistance, the energy imparted on the side plate by the airbag can be equated to the kinetic energy of the side plate;

$$E = \frac{1}{2} I \omega_c^2,$$

where ω_c is the speed at which the plate and bag separate. Figure 18 shows the velocity profile of the side plate during deployment.

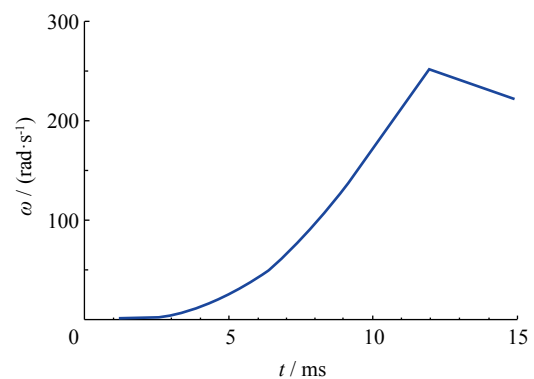


Figure 18 Velocity Profile of Side Plate During Deployment

The maximum speed reached is 250 rad s^{-1} . The rotational moment of inertia of the plate is 0.067. Substituting these values into the kinetic energy equation gives a kinetic energy of 2.094 kJ.

The efficiency of energy transfer from the chemical energy of the sodium azide to the kinetic energy of the side plate can be estimated by treating the airbag a heat engine. Curzon-Ahlborn engine theory gives an approximation for the efficiency of an ideal heat engine with irreversible heat transfer as:

$$\eta = 1 - \sqrt{\frac{T_c}{T_h}},$$

where T_c is the absolute temperature of the heat sink and T_h is the absolute temperature of the heat source. The temperature of the source can be estimated from measurements taken from inflating airbags. Typical peak exhaust temperatures for airbags range from 200 to 500°C [28]. Selecting 200°C as the source temperature and 25°C as the sink temperature, the efficiency is found to be 20.6%. As a conservative estimate, 20% efficiency will be used in this analysis. The amount of sodium azide required is therefore;

$$m \text{ (g)} = \frac{1}{2.16} \frac{2.094}{0.2} = 4.8 \text{ g.}$$

The modest amount of energy required to bring the plate to the required speed can therefore be provided by a small mass of sodium azide. This suggests that the amount of sodium azide used in conventional automotive airbags (typically around 50 g) is more related to the volume of the airbag, and therefore the amount of nitrogen gas required, rather than the amount of energy required. Using smaller volume airbags that inflate quickly and reach very high pressures might, therefore, be more suitable for the side plate application than the conventional high volume airbag used in this analysis. With a more optimized airbag, custom made for the very different task of accelerating the side plate, significant performance improvements may be obtained, such that cheaper materials may be used as a side plate material.

5.3 Power Considerations

As shown in the energy analysis above, the kinetic energy of the plate at max velocity is 2.094 KJ. In terms of power, an average thermal power of 698 kW is required during deployment, assuming 20% thermal efficiency as before.

Explosions are typically very short lasting, high power events. In experiments with sodium azide based mixtures, maximum pressure has been found to occur in just 8 ms [29]. This is consistent with the inflation times of small side curtain airbags.

For larger inflation volumes, it stands to reason that using a greater mass of sodium azide will reduce the inflation time. Releasing the energy contained in 4.8 g of sodium azide in 8ms would give an average thermal power of 1,296 kW. The mass specific power and energy density required by this design is therefore within the order of magnitude offered by modern explosive substances.

6 Conclusion

A head restraint concept designed for lightweight vehicles with tandem seating has been presented in this paper. The concept limits lateral head motion with side plates that rotate downwards from the roof of the vehicle under the force of an inflating airbag. Forward head excursion is reduced by an airbag that fills the cavity between the side plates.

The design satisfies the biomechanical and anthropometric requirements set out in section 4. A consideration of the dynamics of the system has indicated that only by using carbon fibre reinforced polymer as the side plate material can the polar moment of inertia of the side plate be reduced to a level at which deployment with an airbag is practical. The use of airbags supported by webbing that spans rigid frames, instead of solid rigid plates may prove sufficiently light to permit the use of cheaper materials.

Initial analysis has suggested that a deployment time of 15 ms can be achieved with an inflator with four times the inflation rate of a typical frontal airbag. These initial results suggest the design outlined in this paper is feasible and warrants further design optimization. Finite element analysis of the system with a seated dummy model would allow assessment of the effectiveness of the system in reducing injury.

Although this design is targeted specifically at microcars with tandem seating, with further modification of the rotation joints and plate geometry, such a system could potentially find application in vehicles with more conventional seating arrangements.

References / 参考文献

- [1] Sorrell S. Global oil depletion: An assessment of the evidence for a near-term peak in global oil production [R/OL]. (2015-09-01). <http://www.ukerc.ac.uk/publications/global-oil-depletion-an-assessment-of-the-evidence-for-a-near-term-peak-in-global-oil-production.html>.
- [2] Shi Y, Nusholtz G. Effects of Vehicle Mass and Other Parameters on Driver Relative Fatality Risk in Vehicle-Vehicle Crashes [J]. *SAE Int'l J'Transportation Safety*, 2013, 145-165.
- [3] Melvin J, Gideon T. Biomechanical Principles of Racecar Seat Design for Side Impact Protection [R]. *SAE Tech Paper*, 2004-01-3515, 2004.
- [4] Hinch J, Hollowell W T, Kianiantra J, et al. Air bag technology in light passenger vehicles [R]. *National Highway Traffic Safety Administration*, 2001.
- [5] King A I, Yang K H, Zhang L, et al. Is head injury caused by linear or angular acceleration [C]// *Proc IRCOBI Conf*; 2003, Lisbon, Portugal: 1-12.
- [6] Perez J, Palmatier T. Air Bag-Related Fatality in a Short, Forward-Positioned Driver [J]. *Annals of Emergency Medicine*, 1996, 722-724.
- [7] Wetmore J. Engineering with Uncertainty: Monitoring Air Bag Performance [J]. *Sci Eng Ethics Science and Engineering Ethics*, 2008, 201-218.
- [8] Gramling H, Hubbard R. Development of an airbag system for

- FIA formula one and comparison to the HANS head and neck support [R]. **SAE Tech Paper**, 2000-01-3543, 2000.
- [9] Zhang J, Yoganandan N, Pintar F A. Dynamic biomechanics of the human head in lateral impacts [C]// *Proc Ann Adv Automotive Medicine/Ann Sci Conf*, 2009, Baltimore, Maryland: (53) : 249.
- [10] Hubbard R, Begeman P, Downing J. Biomechanical Evaluation and Driver Experience with the Head and Neck Support [R]. **SAE Tech Paper**, 942466, 1994.
- [11] Norman, J. Why Drivers Still Die In Racing Crashes [R/OL]. (2015-09-01). <http://jalopnik.com/why-drivers-still-die-in-racing-crashes-563200728>.
- [12] Society of Automotive Engineers. SAE J1052: Motor Vehicle Driver and Passenger Head Position [S]. 1987.
- [13] Ono K, Ejima S, Kaneoka K et al. Biomechanical response of head/neck/torso and cervical vertebral motion to lateral impact loading on the shoulders of volunteers [J]. *JARI Res J*, 2007, **29**(9): 435-448.
- [14] Gordon C. Anthropometric survey of U.S. army personnel: Methods and summary statistics 1988 [R]. **Defense Technical Information Centre**, ADA225094, 1989.
- [15] Bhise V. Ergonomics in the Automotive Design Process [M]. Boca Raton, FL: CRC Press, 2012.
- [16] OICA. R-point and manufacturer design seat back angle [R/OL]. (2015-09-01). <http://www.unece.org/trans/doc/2006/wp29grsp/HR-06-13e.pdf>.
- [17] Deng B, Melvin J, Rouhana S. Head-neck kinematics in dynamic forward flexion [R]. **SAE Tech Paper**, 983156, 1998.
- [18] Kress T, Porta D, Duma S, et al. A discussion of the air bag system and review of induced injuries [R]. **SAE Tech Paper**, 960658, 1996.
- [19] Huang, M. Vehicle Crash Mechanics [M]. Florida: CRC Press, 2002.
- [20] Friedewald K. Design methods for adjusting the side airbag sensor and the car body [R]. **Volkswagen AG**, 98-S8, 1998.
- [21] Shaw J, Probst E, Donnelly B. Evaluation of the 95th Percentile HIII Large Male Dummy [C/OL]// (2015-09-01). <http://www-nrd.nhtsa.dot.gov/pdf/esv/esv20/07-0228-W.pdf>.
- [22] Matweb. Online materials information resource – Matweb [R/OL]. (2015-09-01). <http://www.matweb.com>.
- [23] Paiva J, Mayer S, Rezende M. Comparison of tensile strength of different carbon fabric reinforced epoxy composites [J]. *Mat Res*, 2006, 83-90.
- [24] Kleiven S, Von H H. Consequences of head size following trauma to the human head [J]. *J Biomechanics*, 2002, **35**(2) : 153-160.
- [25] Smith P A, Wood J R. Poisson's ratio as a damage parameter in the static tensile loading of simple crossply laminates. [J]. *Composites Sci and Tech*, 1990, **38**(1): 85-93.
- [26] Stachowiak G, Batchelor A W. Engineering Tribology [M]. Oxford: Butterworth-Heinemann, 2013.
- [27] Patnaik P. A Comprehensive Guide to the Hazardous Properties of Chemical Substances [M]. New Jersey: John Wiley & Sons, 2007.
- [28] Reed M P, Schneider L W. Skin burns from airbag exhaust gas: laboratory experiments and mathematical modelling [R]. **University of Michigan Transportation Research Institute**, URTMI-94-24, 1994.
- [29] Kishi K, Naganuma, K. Gas-generating agent for air bag [P]. US Patent, No. 4021275, (1977-05-03).